Direct contact membrane distillation: the role of membrane porosity

Isam Janajreh*, Khadije El Kadi, Noora Al Hammadie, Raed Hashaikeh

Mechanical and Materials Engineering Department, Khalifa University of Science and Technology, Masdar Institute P.O. Box 54224, Abu Dhabi, UAE, email: ijanajreh@masdar.ac.ae (I. Janajreh), kelkadi@masdar.ac.ae (K. El Kadi), naalhammadie@masdar.ac.ae (N. Al Hammadie), rhashaikeh@masdar.ac.ae (R. Hashaikeh)

ABSTRACT

Direct contact membrane distillation (DCMD) is pursued as low energy thermally driven process. Its basic configuration consists of two chambers one for the hot brine feed and second for the colder fresh permeate separated by a thin-porous-hydrophobic membrane of low thermal conductivity. The process involves brine evaporation that localized at the hot membrane surface, vapor transport through the thin porous membrane and condensation at the permeate membrane surface side. A sustaining temperature difference across the membrane ensures the driving process pressure. In this work a validated high fidelity model is developed to quantitatively assess the DCMD performance that address the influence of the porosity for homogenous and composite membrane. The flow is governed by the Navier-Stokes of none-isothermal that thermally coupled with the hydrophobic porous membrane consist of a single PVDF layer and a triplet layered membrane in which a stiffer layer SiO$_2$ is sandwiched in between the PVDF to improve membrane post-treatment. The model was tested and run at fixed salinity value for the brine of 4% and inlet temperate of 75°C under different porosity and membrane composite configurations. Results reveals a pronounced influence of the porosity seen by temperature polarization (TPC), mass and heat flux across the membrane, as well as thermal efficiency metrics. Specifically, an increase or decrease in porosity from the baseline 85% by 5 and 10 points lead to and increase/decrease in the mass flux and the thermal efficiency by 11–12% and 22–25%, respectively. The introduction of a sandwiched silicon oxide layer while preserved the same trend and relative values it, however, drastically reduced the mass flux and efficiency due to over all penalty in the membrane conductivity. This suggests that while inclusion of functional material could improve membrane reliability and post treatment one needs to use these materials at higher porosity than the original membrane to compensate for their added conductivity.

Keywords: Membraneporosity; Composite membrane; Membrane distillation; Thermal efficiency; Temperature polarization (TPC)

1. Introduction

Membrane distillation (MD) is a separation method in which a non-wetting, micro-porous membrane is used with a liquid feed flow parallel to one side of the membrane and a condensing, permeate flow on the other, where the process is mainly driven by the temperature difference between both flows. Direct contact membrane distillation (DCMD) is the simplest and most used MD configuration [1]. In MD process, the micro-porous membranes acts as a barrier to liquid solution and allows only the passage of water vapor through it pores due to its hydrophobic nature. A suitable membrane selection for distillation applications should have high porosity and stable mechanical and chemical properties, such properties highly affects the MD performance and mass transfer [2–5]. Membranes are typically made of polymeric and ceramic materials. Still, polymer membranes are the most commonly used for water filtration and distillation processes [6]. Owing to the limitations

*Corresponding author.

in chemical, mechanical, and thermal resistance of polymer membranes, restrictions in using such membranes in various applications is present [7–10]. Polyvinylidene fluoride (PVDF) is one of the most widely used membrane polymer materials in the industry due to its excellent chemical stability mainly antioxidation, good hydrophobicity, higher thermal and hydrolytic stabilities, as well as decent mechanical and membrane forming properties [7,11].

Recent studies of modifications on membrane composition have been conducted to control different processing parameters. Mainly composite membranes are introduced to improve PVDF's hydrophilicity and antifouling due to organic compounds, where hydrophilicity is a favor for many membrane processes. This improvement can be approached by either blending the polymer with inorganic hydrophilic additives or by modifying its chemical and/or physical surface properties using multilayer approach [6]. Yun et al. [7] have prepared and characterized PVDF-SiO$_2$ mixed composite hollow fiber membrane for ultrafiltration (UF) using sol-gel and wet-spinning methods, whereas Zuo et al. [12] have also prepared PVDF composite membrane with SiO$_2$ nanoparticles. Both found that at 2–3 wt.% of SiO$_2$ solution concentration optimal UF performance can be achieved with improved membrane porosity, hydrophilicity, mechanical properties, and anti-fouling performance [7,12]. Yan et al. [13,14] have also synthesized a composite membrane by dispersing alumina nanoparticles (Al$_2$O$_3$) into a PVDF solution for UF, leading to higher hydrophilicity and thus increasing the permeation membrane flux. Though, the addition of alumina nanoparticles did not affect pore size and numbers of the PVDF membrane [13,14].

On the other hand, multilayer composite membrane is widely used in ion-exchange and pervaporation for gas separation [15–18]. Elyashevich et al. [15] proposed a multilayer composite membrane consisting of three layers (polyethylene porous support, conducting polymer, and polymer dopant) to provide a good mechanical support. Higher ion selectivity and membrane hydrophilicity were achieved, thus increasing permeate flux for gas separation [15]. Moreover, Shieh et al. [16] have prepared a novel multilayer composite hollow fiber membrane using silicon rubber, poly(4-vinylpyridine) and porous polysulfone as sealing, selective and support layer, respectively, reaching excellent gas separation performance. Analysis of this novel membrane was done by a resistance model where surface porosity, permeability, and gas separation performance of the multilayer membrane can be evaluated [16].

Different authors have prepared a PVDF multilayer composite membranes for ethanol recovery. For example, Sukitpaneenit and Chung [17] have designed a pore-flow model of a novel dual-layer hollow fibers of PVDF and silica nanoparticles for ethanol recovery by pervaporation. Highly porous support structure with greater hydrophobicity were successfully fabricated, thus accomplishing a very high separation factor [17]. Similarly, Zhan et al. [18] have prepared multilayer PDMS/PVDF/non-woven fiber/PVDF/PDMS composite membrane, enhanced separation performance and permeation rate were achieved.

As noted from literature, composite membrane is very common, flexible, and applicable technology. In our case, a modification of PVDF porous membranes for distillation is intended to overcome the porosity reduction due to heating post-processing. In this work, a multilayer composite membrane is assumed by introducing a conductive silica gel layer in-between two PVDF layers aiming to reach higher porosity, thus higher mass flux coefficient [1]. This approach can highly affect the performance of MD, quantitative comparison between the single- and multi- layer membranes using CFD model are demonstrated in terms of temperature polarization coefficient (TPC), mass flux, and thermal efficiency. These analyses are expected to quantitively assess the role of porosity and composite membrane integration hoping to bring this research closer to the commercialization of the DCMD technology.

2. Materials and methodology

2.1. Experimental validation

Experimental facility is being developed to assess the performance and validate the modeling of DCMD system. Experimentally, however, one is limited in obtaining the overall system performance and with little information on the distribution of the temperature and the concentration or in visualizing the flow which drives the system. High fidelity DCMD modeling provides both the micro- and the macro-scale quantitative system data that enable the designer to reach to optimal design conditions and shorten the lead development time. The experimental facility that was developed to carryout model validation is depicted in Fig. 1 [19–22]. In which a DCMD acrylic module is build which consists of two identical rectangular channels for the brine and the permeate of 210 × 15 × 1 mm separated by the PVDF membrane of known properties per Table 1. The flow to these channels is driven by two peristaltic pumps that inject a uniform laminar flow for the brine and the permeate channels. Each channel is instrumented by 18 T-type thermocouples at an equally distributed distance to records the fluid temperature at the two confiding channel walls as per the schematics in Fig. 1. The system is fed by two reservoir tanks that are kept at fixed temperature by means of a temperature controlling thermostat and stirring propeller. The flux is measured by an overflowing graded TPX flask which connect to the permeate reservoir while the total rejection is measured by recording the initial and final dissolved salt in the permeate side along with the total permeated flux volume.

2.2. Numerical model development

The configuration of flat sheet, even the common fiber tube, DCMD membrane permits one to pursue a reduced 2-D modeling at high resolution. A high fidelity two-dimension computational fluid dynamic (CFD) model is considered as depicted in Fig. 2. The model geometry and setup is built around two channels of 210 × 10 × 1 mm enclosing the thin 130 μm membrane being single or multilayer composite.

Regarding the domain presented in Fig. 2 a steady conjugated heat flow Navier-Stokes system is set to describe the system. This system governing the continuity, the
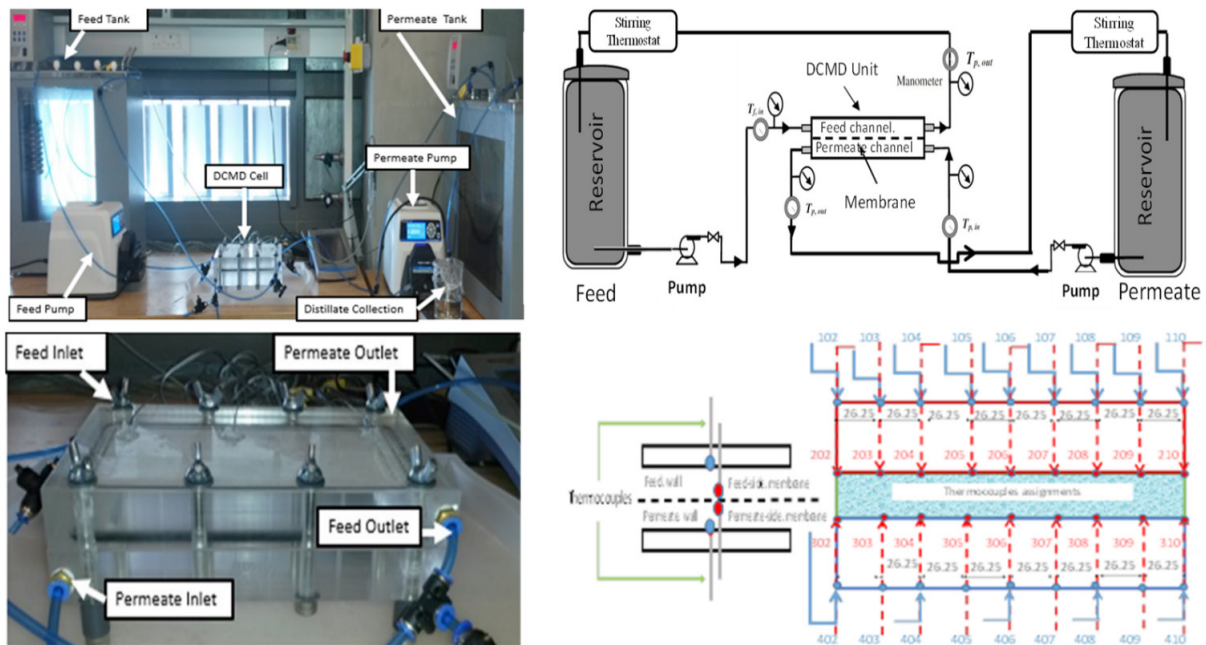
Fig. 1. Experimental module setup and corresponding schematic diagram of the DCMD process along with the fabricated cell unit and thermocouples mounting allocation [19–22].

Table 1
List of the components incorporated in the experimental unit and the membrane physical properties

Parts	Specification
Machined acrylic blocks	Transparent
Hydrophobic membrane	Whole sheet, PVDF-HFP, 130 µm thickness, 0.2 W/m·K conductivity, 42.27 psi liquid entry pressure, 0.15–0.2 µm pore size, electro spinning technology
Pumps	Peristaltic
Calibrated thermocouples	TMQSS-040U-12
Reservoir tanks (40 L capacity)	Electric heater type
Graduated cylinder	TBX (100 mL)
Salinity and pH indicator	Accumet excel XL60 dual channel:
	pH/ion/salinity/conductivity/do meter
Hose and module polyolefin insulation/Thermal cold Inc.	0.032 W/m·K conductivity, –80–100°C operating temp.

x- and y-momentum and energy equations are written in Eqs. (1)–(4) respectively as:

Continuity: $\dfrac{\partial \rho U}{\partial x} + \dfrac{\partial \rho V}{\partial y} = 0$ (1)

x-momentum: $U\dfrac{\partial \rho U}{\partial x} + V\dfrac{\partial \rho U}{\partial y} = -\dfrac{\partial P}{\partial x} + \mu\left(\dfrac{\partial^2 U}{\partial x^2} + \dfrac{\partial^2 U}{\partial y^2}\right)$ (2)

y-momentum: $U\dfrac{\partial \rho V}{\partial x} + V\dfrac{\partial \rho V}{\partial y} = -\dfrac{\partial P}{\partial y} + \mu\left(\dfrac{\partial^2 V}{\partial x^2} + \dfrac{\partial^2 V}{\partial y^2}\right) + \rho g_y$ (3)

Energy: $U\dfrac{\partial \rho C_p T}{\partial x} + V\dfrac{\partial \rho C_p T}{\partial y} = k\left(\dfrac{\partial^2 T}{\partial x^2} + \dfrac{\partial^2 T}{\partial y^2}\right) + S_h$ (4)

where U and V are the velocity components, ρ is the density, μ is the viscosity, g_y is the gravitational acceleration, C_p is the specific heat and k is the thermal conductivity S_h is an additional external heat source or losses that attributed to the latent heat of evaporation at membrane surfaces [23]. A structured quadrilateral mesh type is used to discretize the 2-D flat DCMD baseline that featuring a boundary layer (BL) mesh adjacent to the membrane and channel surface walls. The BL is iteratively set to target a unit normalized wall distance (i.e., $y+ = 1$) to precisely resolve the kinetic/velocity and thermal boundary layers. The mesh size is 2,100 × 64 per channel, 2,100 × 16 for each side of the membrane, and 2,100 × 20 per the Silicon oxide (SiO_2) porous layer.

At the inlet, a flow velocity and temperature, i.e., Dirichlet boundary type, are assigned. The outlet is prescribed

by a zero-velocity gradient and constant atmospheric pressure, i.e., Neumann boundary type. Velocity condition is also assigned to the channel walls in the form of no-slip or penetration condition. Thermally, the outer walls are insulated via zero gradient temperature, i.e., no thermal flux, while the membrane walls are thermally coupled and the temperature is conjugated via Fourier heat flow equation. These conditions are shown in Fig. 2b cutaway of the developed baseline mesh. The nominal flow conditions for the brine/feed and fresh/permeate are set at Reynolds number of 10 and 100, which is equivalent to 0.01 m/s and 0.1 m/s, respectively. The nominal temperature for the feed is set at 75°C while for the permeate is set at 25°C. Table 2 addresses the initial and boundary conditions of all faces and interfaces of the DCMD model. Eqs. (1)–(4) are solved using the commercial CFD Ansys-FLUENT which is based on the finite volume and segregated solver formulation following the semi-implicit method for pressure-linked equations (SIMPLE) for the pressure-velocity coupling. The second order upwind discretization scheme is employed for spatial derivatives properties. The convergence criterion is set at 1×10^{-12} residuals for the continuity, the two momentums and the energy scalar equations. Temperature distribution resulted from the solution of the system which forms the basis of all system metrics including mass flux, thermal efficiency and the temperature polarization coefficient.

2.3. System metric evaluation

The transport of mass across the porous membrane is driven by the computed temperature gradient across the membrane surface and is evaluated outside the CFD conjugated flow model. The molecular diffusion theory has been successfully followed for the DCMD studies as described elsewhere [24–27]. This flux is expressed as:

$$J'' = c_m \left(P_f^{sat} - P_p^{sat} \right) \tag{5}$$

where c_m is the combined mass coefficient whereas p_f and p_p are respectively the membrane surface water vapor pressures at the feed and permeate channel. These latter pressures are described per the monotonic Antoine equation [28] for pure water, and is adjusted for saline/waste water in function with the brine concentration and water activity [20–22,29–30], is written as:

$$P_{i(pure)}^{sat}(T) = \exp\left(23.1964 - \frac{3816.44}{Tm - 46.13} \right), \ i \in \{f, p\} \tag{6}$$

The combine coefficient c_m accounts for several flow physics such as Knudson that based on the mean free path, molecular diffusion, and Poiseuille pressure driven flow [31–33]. Following Chen et al. [25,34] and the authors work a combined Knudson and Poiseuille model is adopted [19–22] and is written as:

$$c_m = c_k + c_p = 1.064\alpha(T)\frac{\varepsilon r}{\tau\delta_m}\sqrt{\frac{M_w}{RT_{mt}}} + 0.125\beta(T)\frac{\varepsilon r^2}{\tau\delta_m}\frac{M_w P_m}{RT_{mt}\mu_v} \tag{7}$$

Where $\alpha(T)$, and $\beta(T)$ respectively the Knudsen diffusion and Poiseuille flow models contributions. M_w is molar mass of the water in (kg/mol), T_{mt} is mean membrane
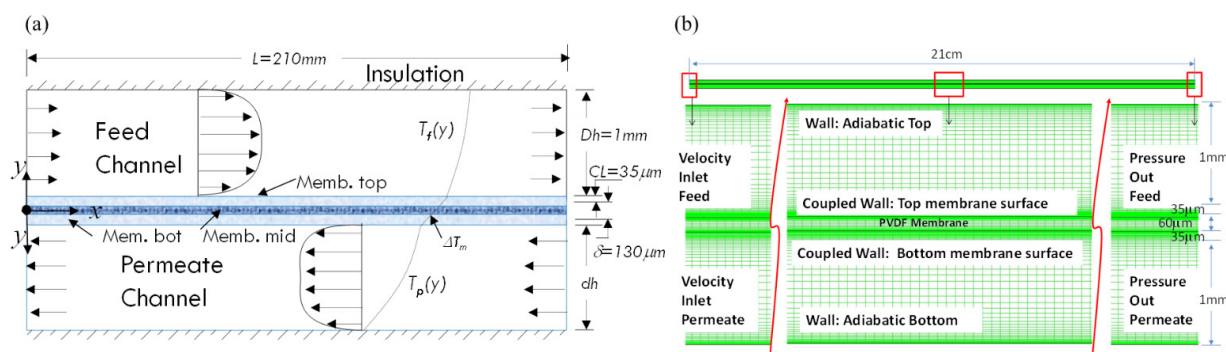
Fig. 2. (a) Schematic diagram for the baseline parallel flow of DCMD cofiguration and (b) the model descritization mesh.

Table 2
Summary of the initial and boundary conditions for the DCMD model

Boundary conditions		Feed channel	Permeate channel	Airgap channel
Inlet channel	*Kinetic*	0.01/0.1 m/s	0.01/0.1 m/s	0.01/0.1 m/s
	Thermal	75°C	25°C	25°C
Outlet channel		Zero pressure, dV/dx = 0	Zero pressure, dV/dx = 0	Zero pressure, dV/dx = 0
Upper wall *Thermal*	*Kinetic*	Stationary/No-slip	Stationary/No-slip	Stationary/No-slip
	Zero heat flux (insulated)	Coupled	Coupled	
Lower wall *Thermal*	*Kinetic*	Stationary/No-slip	Stationary/No-slip	Stationary/No-slip
	Coupled	Zero heat flux (insulated)	Coupled	

temperature (°C), R is gas constant, P_m is mean pressure, δ_m thickness of the membrane, μ_v is gas viscosity, r is pores radius, ε is porosity of the membrane, and τ is tortuosity. This latter factor is taken to be the reciprocal of the pores as in the work of Iversen et al. [35] and leaving the mass flux proportional to the square of the porosity. This model flux was also experimentally validated and was shown to be directly proportional with the increase in the pore size and porosity while inversely proportional with the membrane tortuosity and thickness [19–21].

The temperature polarization coefficient (TPC) is very common and popular metrics which is directly read from the computed CFD temperature. It is defined as the ratio of boundary layer resistance to the bulk heat transfer resistance which is simply written as:

$$TPC = \frac{\Delta T_m}{\Delta T_b} = \frac{T_{m,f} - T_{m,p}}{T_{b,f} - T_{b,p}} \tag{8}$$

where the subscripts m, b, f, and p are respectively signify the membrane, the bulk, the feed and the permeate flow. A high theoretical value is sought 0.7 or so. High TPC value hinder the DCMD system to operate in mass flux limited range particularly when the membrane poses high permeability whereas low TPC value confine the operation of the system to operate in limited heat transfer condition. The latter occurs when the membrane possess a high thermal conductivity [19].

Membrane heat (Q_m) is gained through convective at the feed side with the surrounding fluid which equated to the transmembrane heat flux that comprises a conductive (Q_c) and a latent heat (Q_m) through the membrane, before it lost again through convective once again at the permeate side. These are described per Fig. 3 where Fourier heat law is invoked.

Similarly, an enthalpy temperature relation does exist through which the latent heat is evaluated following Termpiayakul [36] these equations are written as:
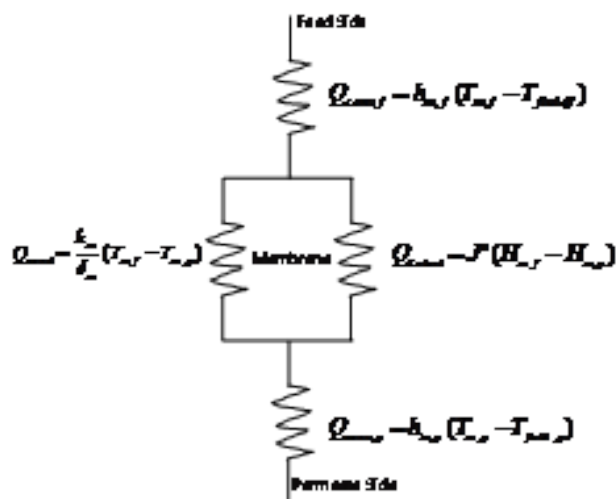
Fig. 3. The heat transfer within the membrane, and denote the enthalpy and membrane thickness, and is the weighted membrane conductivity the subscripts f and p signify the feed and permeate.

$$H_{m,i} = 1.7535\left(T_{m,i}\right) + 2024.3, \qquad i \in \{f,p\} \tag{9}$$

$$Q_v = J''\Delta H = J''\left(H_{m,f} - H_{m,p}\right) \tag{10}$$

where the $T_{m,i}$ and $H_{m,I}$ is the membrane surface temperature and enthalpy and the subscript f and p denote the feed, and permeate sides. J'' is the mass flux. This heat per Fig. 3 initially is convicted to the feed membrane surface and then crosses the membrane in the form of a combined conductive and latent heat of evaporation, and eventually is convicted once again at permeate membrane surface [25,29]. It should be noted that the model accounts for the total heat through the membrane as conductive heat initially that conserves the heat balance. This heat then is split between conductive and latent heat per the mass computed in Eq. (5). It was shown in earlier work of the authors that further iterative coupling on the mass flux and temperature lead to insignificant change in the computed temperature values [37]. The split between the conduction and latent heat enable one to evaluate the thermal efficiency metric which is defined as the fraction of the latent heat of evaporation that otherwise lost in the conduction to the total heat and is written as:

$$\eta = \frac{Q_v}{Q_v + Q_c} \tag{11}$$

Summary of the thermodynamics properties of the PVDF membrane, the brine and fresh water in each circulating channels are listed in Table 3.

2.4. Assessment of the role of porosity

Pressure drop through porous membrane is commonly modeled following both a permeability and an inertial loss coefficients [41], and is commonly written as:

$$\frac{\Delta p}{\delta} = \frac{\mu}{\alpha}v_{mean} + C_2 \frac{1}{2}\rho v_{mean}^2 \tag{12}$$

where δ is the membrane/porous media thickness, α is the permeability (with length unit), μ is the gas/vapor viscosity, ρ is the vapor density, C_2 is the permeability. Ergun used a semi-empirical correlation for backed beds that applicable over long range of flow velocity which described as [42]:

$$\frac{\Delta p}{\delta} = \frac{150\mu}{D_p^2}\frac{\left(1-\varepsilon\right)^2}{\varepsilon^3}v_{mean} + \frac{1.75\rho}{D_p}\frac{\left(1-\varepsilon\right)}{\varepsilon^3}v_{mean}^2 \tag{13}$$

where is the porosity and D_p the particle size (water molecule size 2.75 A) which is in the same order of the membrane pore size. Because DCMD system is proceeds in laminar (Re≈100) regime, flow is confined in a small thickness and low velocity, the inertia (2nd) term in Eqs. (12) and (13) can be dropped as presented by the Darcy equation or the Black-Kozeny equation, respectively. To investigate the role of porosity the semi-empirical pressure difference ($P_f - P_p$) in Eq. (5) can be adjusted to account for the additional pressure loss due to porosity. Alternatively, one can adjust the pressure coefficient (c_m) per Eqs. (5) and (7). The

Table 3
Properties of the of membrane and two sides of the flow materials

Material	Density (kg/m³)	Specific heat (J/kg·K)	Conductivity (W/m·K)	Viscosity (Pas)
PVDF [38]	1,175	1,325	0.2622	–
Vapor	0.554	2,014	0.0261	–
Membrane	302.2	1,896.9	0.0662	–
Silica [40]	2300	1130	1.5	–
Saline sea water* [39]	1013.2	4064.8	0.642	5.86E-4
Pure water** [30]	995.2	4182.1	0.613	8.38E-4

*At 4% salinity and 323 K; **At 303 K.

c_m is proportional to the square of porosity under Ervin's assumption of the tortuosity value ($\tau = 1/\varepsilon$). This would change the mass flux and hence an updated latten heat calculated from the total transmembrane heat flux. Five values sweep for the porosity is evaluated to quantify and assess its role on the transmembrane mass flux and the thermal efficiency.

3. Results and discussion

3.1. Model validation

Model validation is carried out by comparing the temperature measurements of the channel and membrane surfaces which are readily available following several minutes of induction period of the system presented in Fig. 1. The values of the thirty-six spatially located thermocouples and their corresponding numerical values are depicted in Fig. 4. The TPC also is evaluated for the two data, i.e., experimental measurements and numerical simulation. As can be seen in the Fig. 4 there is a good agreement in the measured and computed temperature distribution as well as in the TPC values. It should be noted that the validation took place at 50°C and 25°C for the feed and permeate flow temperatures, respectively and at peristaltic pump mass flow rate following laminar regime, i.e., Re = 50 and in counter-flow configuration. Authors recent work also showed the evolution of the permeated mass flux through the membrane and monitored the conductivity at permeate side [43]. Although the condition were not exactly at the same inlet temperatures, i.e., 48°C and 25°C, a flux of 0.00194 kg/m².s was obtained and a constant conductivity of 140 mS/cm was observed over the course of experiments that lasted several hours which confirmed near 100% salt rejection of these DCMD membranes.

Furthermore, confirmation is can be seen in the contours of computed temperature and pressure distribution depicted in Fig. 5. The figure is stretched in the vertical direction to facilitate the visualization. It shows the vertical temperature variation in the individual channel due to the coupled membrane and insulated outer channel. It also shows the axial pressure drop due to channel friction and losses that add to 25.6 Pascal. This is the computed pressure under the prescribed zero gage pressure at each channel inlet. As Navier-Stokes equation is 1st order differential in terms of pressure, the naturally imposed zero value at the exist is sufficient and sets the pressure reading in the gauge scale.
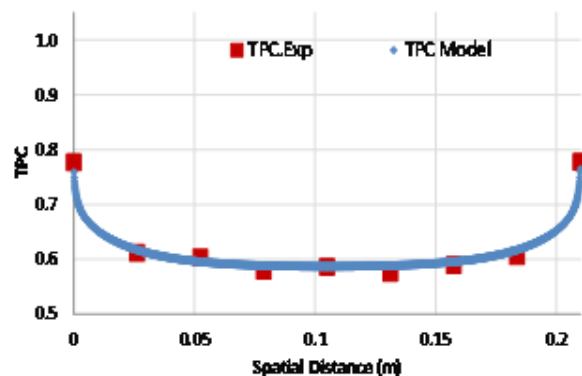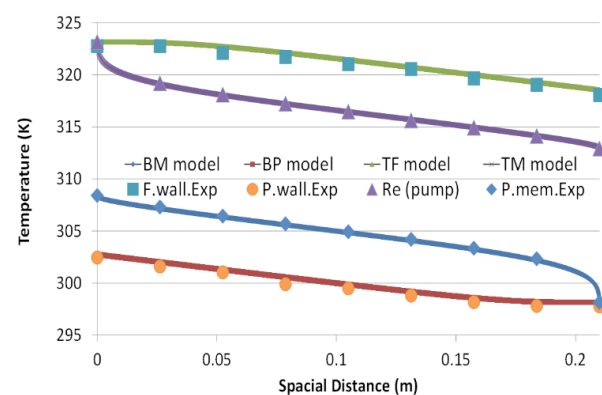
Fig. 4. Counter flow experimental and numerical model results of the surface temperature and the inferred TPC value.

3.2. Composite membrane analysis

It has been mentioned that integration of a porous stiff layer in between the membrane can lead to substantial improvement in membrane manufacturing and reproducibility that further enhances its performance. Moreover, it was observed that electrospun membrane endures in inconstancy in thickness and porosity to some extent. This issue alleviated through post-processing via hot pressing which comes at price in reducing the overall membrane porosity. The thought of inclusion high porous and a stiffer material in between, that preferably characterized with low thermal conduction, would resolve this problem. This is the idea
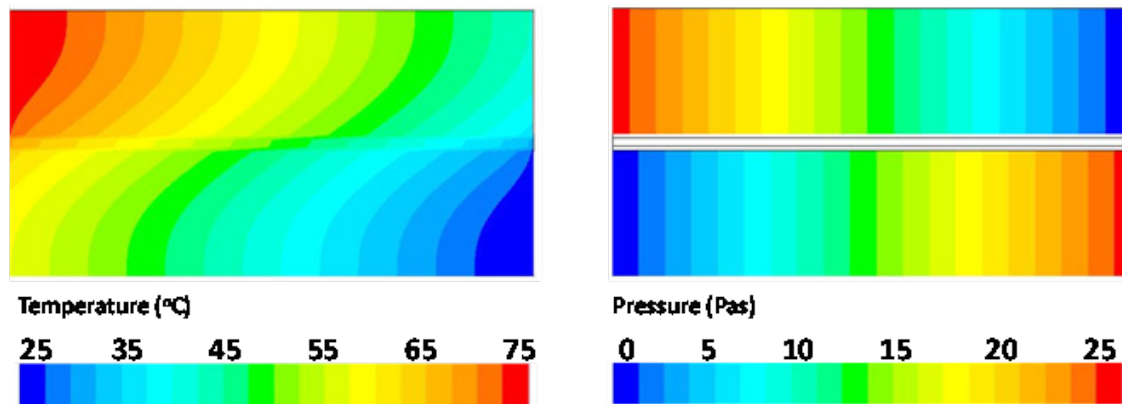
Fig. 5. Counter flow numerical model results of the channels temperature and pressure distributions (the y-coordinate is 50× scaled for better visualization).

behind the design of composite membrane in this work. The computed TPC values for the homogenous and composite membrane assuming both have similar thickness (130 mm) and same porosity (ε = 85%) is shown in Fig. 6. It is obvious that the composite membrane attained a lesser value than the bare PVDF membrane and that are obtained at two values of mass flow (Reynolds number 10 and 100) through the channels for the feed and permeate. The shape of the TPC curve in the streamline of the flow is left and right symmetrical at the middle stream and reaching as high as 0.65 for the bare PVDF membrane and 0.55 for the composite membrane at Re 10 and 0.72 and 0.61 at Re 100. Their average values are respectively 0.59 for the PVDF and 0.44 for the composite at Re 100 while 0.55 and 0.40 at Re 10. It should be noted that the TPC value for composite membrane at low Re is approaching the heat limited range of operation of the DCMD signifying low performant membrane.

The results of the mass flux for the homogenous and composite membrane assuming both has at the same thickness (130 mm) and same porosity (ε = 85%) is shown in Fig. 7. As can be seen from the figure the homogenous membrane seems to yield a higher mass flux in comparison to the composite averaging 0.0058 kg/m²·s vs. 0.0036 kg/m²·s at Re 10 and 0.0137 kg/m²·s vs. 0.0099 kg/m²·s at Re 100. Although the SiO$_2$ insertion is deemed necessary for membrane post-treatment, the loss in mass flux is recognized by the higher thermal conductivity of the integrated SiO$_2$ layer which is nearly 20-fold more than the bare PVDF. It should be noted that the thickness in the composite is distributed 35, 60, and 35 mm for the PVDF, SiO$_2$, and PVDF layers, respectively.

The thermal efficiency of these membrane also evaluated and are depicted in Fig. 8. The highest attained efficiency is near 80% at entry of the hot bine feed and is in the favor once again of the bare PVDF membrane which is attributed to its lower conductivity. Similarly, at higher Reynolds number the influence is exasperated, i.e., averaging respectively 47.23% and 19.10% for the homogenous and composite membrane at Re 100, and 20.20% and 6.95% at Re 10.

3.3. Role of membrane porosity

The mass flux for five common values of the porosity are depicted in Fig. 9 for both the homogenous and
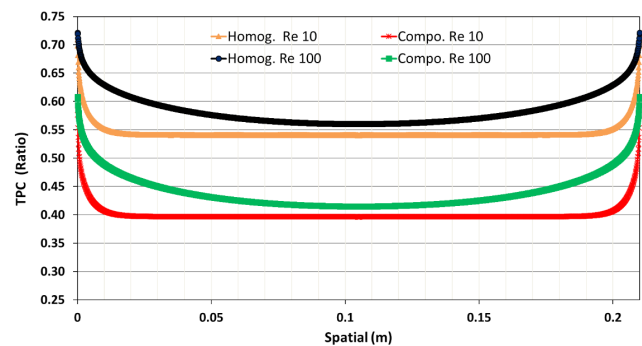
Fig. 6. Homogenous and triplet layer composite membrane TCP values at Re = 10 and 100 and porosity 85%.
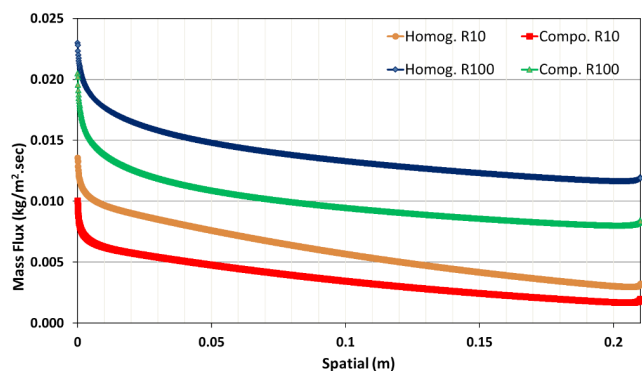
Fig. 7. Homogenous and triplet layer composite membrane mass flux at Re = 10 and 100 and porosity 85%.

composite membrane. The trend is clearly demonstrated in the attained mass flux which is directly proportion to the porosity value. The composite membrane also shows similar trend but at lower starting value from the baseline. The results indicates a 5% gain or loss in the porosity will lead to nearly 11–12% increase in the mass flux. The average values are also tabulated for both membranes as listed in Table 4. It should be noted that the gain/loss for the two membranes is identical since the porosity is accounted for
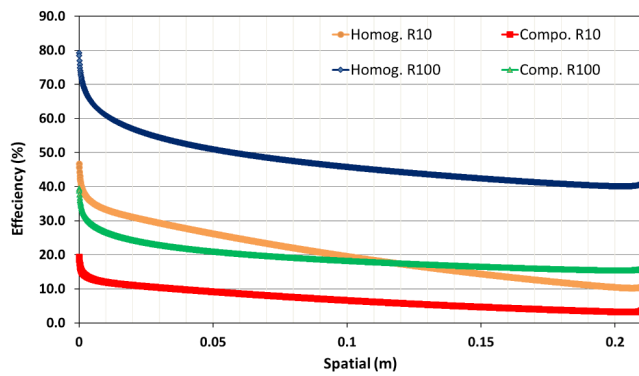
Fig. 8. Homogenous and three-layer composite membrane thermal efficiency at Re = 10 and 100 and porosity 85%.
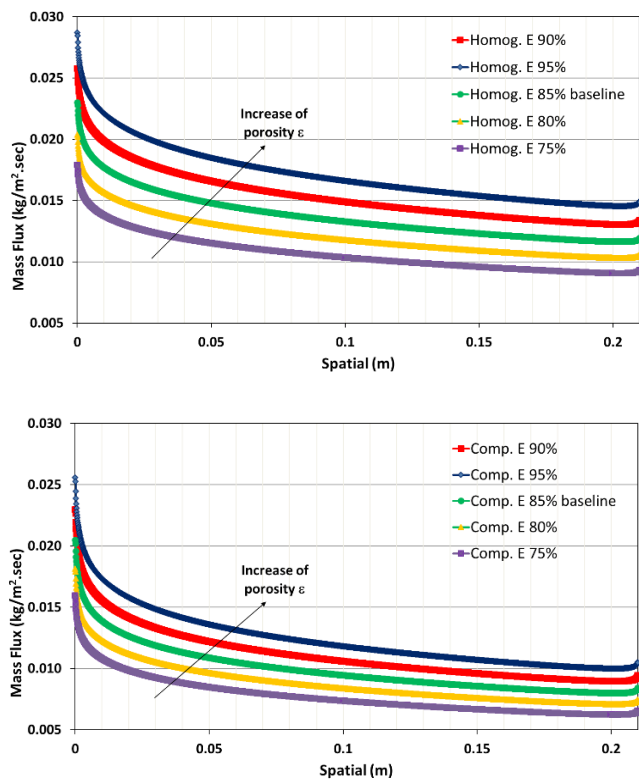
Fig. 9. Mass flux at Re = 100 and different porosity values, ε {75–95%}, left – homogenous membrane, and right – triplet layer composite membrane.

similarly as per Eq. (7) which lead to a 2nd order polynomial dependency when the tortuosity is also considered equal to the reciprocal of the porosity.

The thermal efficiency for the common values of the porosity are shown in Fig. 10 for both membranes. A similar proportionality trend is observed with the increase of the porosity value. The composite membrane reflects the same trend however the corresponding baseline values are at much lower efficiency than the homogenous. The results show a gain 5% change in the porosity will lead to nearly 11–12% change in the thermal efficiency. Table 5 list these values where the gain/loss for the two membranes is identical.

Table 4
Average mass flux values at Re = 100 and different porosity values for the homogenous and composite membranes

	Homogenous		Composite	
(%)	J″ (kg/m²·s)	Gain/loss (%)	J″ (kg/m²·s)	Gain/loss (%)
75	0.010663317	–22.1451	0.007715	–22.1451
80	0.012132486	–11.4184	0.008778	–11.4184
85	0.013696439	baseline	0.009910	baseline
90	0.015355177	12.11104	0.011110	12.11104
95	0.017108700	24.91385	0.012378	24.91385
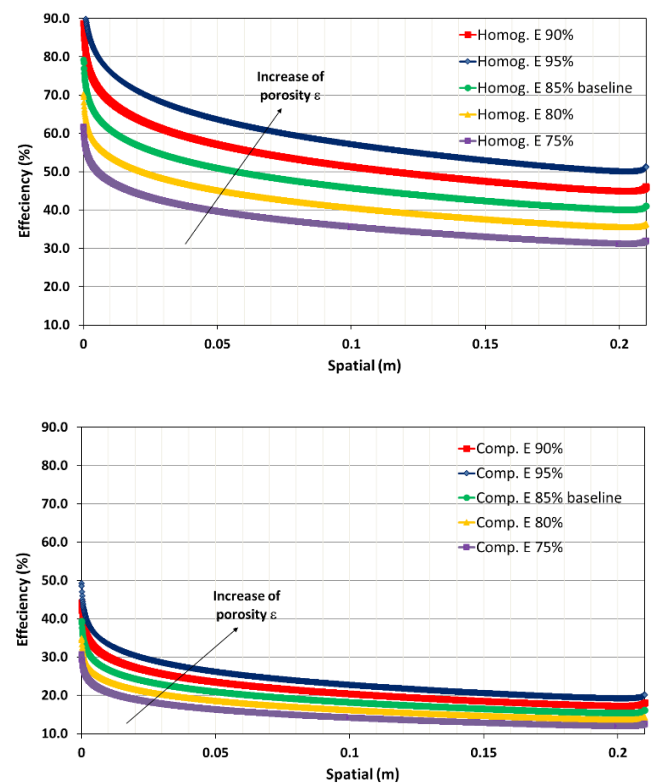
Fig. 10. Thermal Efficiency at Re = 100 and different porosity values, e{75–95%}, left – homogenous membrane and right – triplet layer composite membrane.

Table 5
Average thermal efficiency values at Re = 100 and different porosity values for the homogenous and composite membranes

	Homogenous		Composite	
(%)	(%)	Gain/loss (%)	(%)	Gain/loss (%)
75	36.77078127	–22.1453	14.86716	–22.1453
80	41.8369778	–11.4187	16.91552	–11.4187
85	47.23002572	baseline	19.09604	baseline
90	52.94992503	12.11073	21.4087	12.11073
95	58.99667573	24.91349	23.85353	24.91349

4. Conclusion

The direct contact membrane distillation (DCMD) is characterized with low energy thermally driven process that can be utilized for, hydrocarbon gas separation, water purification and desalination, and juice concentration. In this work, a validated high fidelity model is developed to quantitatively assess the DCMD performance that address two parameters, namely the integration of metal oxide thin layer for membrane composite and the role of porosity. The composite membrane thought to facilitate manufacturing and tighten the resulted wide property range. The flow is governed by the Navier-Stokes of non-isothermal thermally coupled flow with the hydrophobic porous membrane consist of single layer as well as an improved triplet layers' membrane. The model is generic to account for the variable operating conditions (temperature, velocity, brine salinity) and membrane properties (porosity, conductivity, thickness). The model was tested and run at fixed salinity value for the brine of 4% and inlet temperate of 75°C under different porosity and membrane composite configurations. Results reveals a pronounced influence of the porosity seen by the mass flux across the membrane and the thermal efficiency metrics. Particularly, an increase or decrease in porosity from the baseline 85% by 5 and 10 points lead to and increase/decrease in the mass flux and the thermal efficiency by 11–12% and 22–25%, respectively. The introduction of a sandwiched silicon oxide layer, while preserved the same trend and relative values, it drastically reduced the mass flux and efficiency due to overall penalty in the membrane conductivity. This suggests that when inclusion of functional material to improve membrane reliability and post treatment, one need to target a high porosity beyond the original membrane as well as lower conductivity if possible.

Acknowledgments

References

[1] I. Janajreh, D. Suwwan, R. Hashaikeh, Theoretical and experimental study of direct contact membrane distillation, Desal. Water Treat., 57(33) (2016) 15660–15675.

[2] M. Gryta, Influence of polypropylene membrane surface porosity on the performance of membrane distillation process, J. Membr. Sci., 287 (2007) 67–68.

[3] M. Khayet, A. Velazquez, J.I. Mengual, Modeling mass transfer through a porous partition: effect of pore size distribution, J. Non-Equilib. Thermodyn., 29 (2004) 279–299.

[4] M. Khayet, T. Matsuura, Pervaporation and vacuum membrane distillation processes: modeling and experiments, AIChE J., 50 (2004) 1697–1712.

[5] J. Phattaranawik, R. Jiraratananon, A.G. Fane, Effect of pore size distribution and air flux on mass transport in direct contact membrane distillation, J. Membr. Sci., 215 (2003) 75–85.

[6] M. Padaki, R. Surya Murali, M.S. Abdullah, N.Misdan, A. Moslehyani , M.A. Kassim, N. Hilal, A.F. Ismail, Membrane technology enhancement in oil–water separation. A review, Desalination, 357 (2015) 197–207.

[7] L.-Y. Yu, Z.-L. Xu, H.-M. Shen, H. Yang, Preparation and characterization of PVDF–SiO$_2$ composite hollow fiber UF membrane by sol–gel method, J. Membr. Sci., 337 (2009) 257–265.

[8] A.V.R. Reddy, D.J. Mohan, A. Bhattacharya, et al., Surface modification of ultrafiltration membranes by pre-adsorption of a negatively charged polymer. I. Permeation of water soluble polymers and inorganic salt solutions and fouling resistance properties, J. Membr. Sci., 214 (2003) 211–221.

[9] Z.L. Xu, T.S. Chung, K.C. Loh, et al., Polymeric asymmetric membranes made from polyetherimide/polybenzimidazole/poly(ethylene glycol) (PEI/PBI/PEG) for oil–surfactant–water separation, J. Membr. Sci., 158 (1999) 41–53.

[10] Z.L. Xu, T.S. Chung, Y. Huang, Effect of polyvinylpyrrolidone molecular weights on morphology, oil/water separation, mechanical and thermal properties of polyetherimide/polyvinylpyrrolidone hollow fiber membranes, J. Appl. Polym. Sci., 74 (1999) 2220–2233.

[11] D. Hou, J. Wang, D. Qu, Z. Luan, X. Ren, Fabrication and characterization of hydrophobic PVDF hollow fiber membranes for desalination through direct contact membrane distillation, Sep. Purif. Tech., 69 (2009) 78–86.

[12] X. Zuo, S. Yu, X. Xu, J. Xu, R. Bao, X. Yan, New PVDF organic–inorganic membranes: The effect of SiO2 nanoparticles content on the transport performance of anion-exchange membranes, J. Membr. Sci., 340 (2009) 206–213.

[13] L. Yan, Y. Li, C.B. Xiang, Preparation of polyvinylidene fluoride (pvdf) ultrafiltration membrane modified by nano-sized alumina (Al2O3) and its antifouling research, Polymer, 46 (2005) 7701–7706.

[14] L. Yan, Y. Li, C. B. Xiang, S. Xianda, Effect of nano-sized Al$_2$O$_3$-particle addition on PVDF ultrafiltration membrane performance, J. Membr. Sci., 276 (2006) 162–167.

[15] G.K. Elyashevich, E.Y. Rosova, I.S. Kuryndin, Properties of multi-layer composite membranes on the base of polyethylene porous films, Desalination, 144 (2002) 2 l–26.

[16] J. Shieh, T-S. Chung, D.R. Paul, Study on multi-layer composite hollow fiber membranes for gas separation, Chem. Eng. Sci., 54 (1999) 675–684.

[17] P. Sukitpaneenit, T-S. Chung, PVDF/nanosilica dual-layer hollow fibers with enhanced selectivity and flux as novel membranes for ethanol recovery, Ind. Eng. Chem. Res., 51 (2012) 978–993.

[18] X. Zhan, J. Li, J. Huang, C. Chen, Enhanced pervaporation performance of multi-layer PDMS/PVDF composite membrane for ethanol recovery from aqueous solution, Appl. Biochem. Biotechnol., 160 (2010) 632–642.

[19] I. Janajreh, D. Suwwan, R. Hashaikeh, Assessment of direct contact membrane distillation under different configurations, velocities and membrane properties, Applied Energy, 185 (2017) 2058–2073.

[20] I. Janajreh, D. Suwwan, Numerical simulation of direct contact membrane desalination (DCMD): II, Int. J. Eng. Res. Innov., 6 (2014) 21–33.

[21] I. Janajreh, D. Suwwan, Numerical simulation of direct contact membrane desalination in conjugate heat transfer configuration: role of membrane conductivity, Int. J. Sustain. Water Environ. Syst., 6 (2014) 81–87.

[22] I. Janajreh, D. Suwwan, H. Fath, Flow analysis of low energy direct contact membrane desalination, Int. J. Therm. Environ. Eng., 8 (2014) 133–138.

[23] H. Yu, X. Yang, R. Wang, A.G. Fane, Numerical simulation of heat and mass transfer in direct membrane distillation in a hollow fiber module with laminar flow. J. Membr. Sci., 384 (2011) 107–116.

[24] L.F. Greenlee, D.F. Lawler, B.D. Freeman, B. Marrot, P. Moulin, Reverse osmosis desalination: water sources, technology, and today's challenges, Water Res., 43 (2009) 2317–2348.

[25] T.-C. Chen, C.-D. Ho, H.-M. Yeh, Theoretical modeling and experimental analysis of direct contact membrane distillation. J. Membr. Sci., 330 (2009) 279–287.

[26] B.L. Pangarkar, M.G. Sane, Heat and mass transfer analysis in air gap membrane distillation process for desalination, Membr. Water. Treat., 2 (2011) 159–73.

[27] Z. Jin, D. Yang, S. Zhang, X. Jian, Hydrophobic modification of poly(phthalazinone ether sulfone ketone) hollow fiber membrane for vacuum membrane distillation, J. Membr. Sci., 310 (2008) 20–27.

[28] A. Bahmanyar, M. Asghari, N. Khoobi, Numerical simulation and theoretical study on simultaneously effects of operating parameters in direct contact membrane distillation, Chem. Eng. Process. Intensif., 61 (2012) 42–50.

[29] M. Khayet, Membranes and theoretical modeling of membrane distillation: A review, Adv. Colloid Interface Sci., 164 (2011) 56–88.

[30] K.W. Lawson, D.R. Lloyd, Membrane distillation. II. Direct contact MD, J. Membr. Sci., 120 (1996) 123–133.

[31] Z. Ding, L. Liu, M.S. El-Bourawi, R. Ma, Analysis of a solar-powered membrane distillation system, Desalination, 172 (2005) 27–40.

[32] V.A. Bui, L.T.T. Vu, M.H. Nguyen, Modelling the simultaneous heat and mass transfer of direct contact membrane distillation in hollow fiber modules, J. Membr. Sci., 353 (2010) 85–93.

[33] A.O. Imdakm, T. Matsuura, Simulation of heat and mass transfer in direct contact membrane distillation (MD): the effect of membrane physical properties, J. Membr. Sci., 262 (2005) 117–128.

[34] T.-C. Chen, C.-D. Ho, Immediate assisted solar direct contact membrane distillation in saline water desalination, J. Membr. Sci., 358 (2010) 122–130.

[35] S.B. Iversen, V.K. Bhatia, K. Dam-Johansen, G. Jonsson, Characterization of microporous membranes for use in membrane contactors, J. Membr. Sci., 130 (1997) 205–217.

[36] P. Termpiyakul, R. Jiraratananon, S. Srisurichan, Heat and mass transfer characteristics of a direct contact membrane distillation process for desalination, Desalination, 177 (2005) 133–141.

[37] I. Janajreh, D. Suwwan, R. Hashaikeh, Coupled modelling of membrane desalination, Int. Conf. of Waste and Wastewater Treatment and Valorization, Athens, Greece, 2015.

[38] B.S. Sparrow, Empirical equations for the thermodynamic properties of aqueous sodium chloride, Desalination, 159 (2003) 161–70.

[39] "Silica - Silicon Dioxide (SiO_2)." AZoM.com. N.p., 27 May 2016. Web.

[40] C.L. Yaws, Chemical properties handbook: physical, thermodynamic, environmental, transport, safety and health related properties for organic and inorganic chemicals, 1999.

[41] I. Janajreh, A. Hasania, H. Fath, Numerical simulation of vapor flow and pressure drop across the demister of MSF desalination plant, E. Conv. and Manag., 65 (2013) 793–800.

[42] S. Ergun, Fluid flow through packed columns, Chem. Eng. Prog. 48 (1952) 89–94.

[43] B. Lalia, I. Janajreh, R. Hashaikeh, A facile approach to fabricate superhydrophobic membranes with low contact angle hysteresis, J. Membr. Sci., 539 (2017) 144–151.